BOLETIN DE LA SOCIEDAD ESPAÑOLA DE
Cerámica y Vidrio
www.elsevier.es/bsecv

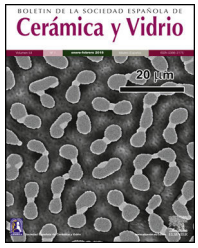

Enhancing NiZn ferrite properties through microwave sintering: A comparative study

Carolina Clausell-Terol[a,*], *Antonio Barba-Juan*[a], *Andres Mormeneo-Segarra*[a], *Piotr Putyra*[b], *Lucyna Jaworska*[c]

[a] *Departamento de Ingeniería Química, Instituto Universitario de Tecnología Cerámica, Universitat Jaume I, 12071 Castellón de la Plana, Spain*
[b] *Krakow Institute of Technology, Zakopiańska 73, 30-418 Krakow, Poland*
[c] *Faculty of Non-Ferrous Metals, AGH University of Krakow, 30-059 Krakow, Poland*

ARTICLE INFO

Article history:
Received 19 June 2023
Accepted 18 October 2023
Available online 3 November 2023

Keywords:
Magnetic permeability
Microwave sintering
Nanoparticulated ferrite
Ni–Zn ferrite

ABSTRACT

The structural, microstructural, morphological, and electromagnetic properties of a micro- and nanostructured nickel–zinc ferrite ($(Cu_{0.12}Ni_{0.23}Zn_{0.65})Fe_2O_4$) were studied after sintering between 900 and 1100 °C. The microparticulated ferrite (MICRO) was a commercial material, while the nanoparticulated ferrite (NANO) was obtained through high energy milling of the former. The effect of microwave heating (MW), compared to traditional infrared sintering (IR), was investigated.

Microwave sintering successfully controlled the grain growth of both granulometries and produced sintered bodies with high relative densities (low porosity), small average grain size, narrow grain size distribution, and a high value of the complex magnetic permeability-imaginary part (μ'') for the MICRO ferrite. In the case of the NANO ferrite, microwave sintering yielded values similar to those obtained by conventional IR.

Microwave sintering significantly affected the densification and grain growth processes for both granulometries studied. Additionally, reducing the granulometry of the starting ferrite powder had a noticeable impact on the microstructure and electromagnetic properties of the sintered ferrites, regardless of whether microwave or infrared radiation was used. However, the magnetic property (μ'') decreased when the particle size of the starting powder was reduced from micro to nanometric scale, irrespective of the sintering source. This observation is supported by our previously published mathematical models that establish relationships between the complex magnetic permeability, magnetization mechanisms, angular frequency, and ferrite microstructure.

* *Corresponding author.*
E-mail address: cclausel@uji.es (C. Clausell-Terol).
https://doi.org/10.1016/j.bsecv.2023.10.003

Mejora de las propiedades de la ferrita de NiZn mediante sinterización por microondas: un estudio comparativo

Palabras clave:
Ferrita de Ni-Zn
Ferrita nanoestructurada
Permeabilidad magnética
Sinterización por microondas

RESUMEN

Se estudiaron las propiedades estructurales, microestructurales, morfológicas y electromagnéticas de una ferrita de níquel-zinc micro y nanoestructurada ($[Cu_{0.12}Ni_{0.23}Zn_{0.65}]Fe_2O_4$) tras su sinterización en el intervalo 900-1100°C. La ferrita microparticulada (MICRO) era un material comercial, mientras que la nanoparticulada (NANO) se obtuvo por molienda de alta energía de la primera. Se investigó el efecto del calentamiento por microondas (MW), en comparación con la sinterización tradicional por infrarrojos (IR).

La sinterización por MW controló eficazmente el crecimiento de grano de ambas granulometrías y produjo piezas sinterizadas de alta densidad relativa (baja porosidad), un tamaño medio de grano pequeño, una distribución de tamaños de grano estrecha y un alto valor de la parte imaginaria de la permeabilidad magnética compleja (μ''), para la ferrita MICRO. En el caso de la NANO, la sinterización por MW condujo a valores similares a los obtenidos por la sinterización convencional por IR.

La sinterización por MW afectó significativamente los procesos de densificación y crecimiento de grano para ambas granulometrías estudiadas. Además, reducir la granulometría del polvo de ferrita de partida tuvo un impacto notable en la microestructura y propiedades electromagnéticas de las ferritas sinterizadas, independientemente de si se utilizó radiación por MW o IR. Sin embargo, la propiedad magnética (μ'') disminuyó cuando el tamaño de partícula del polvo de partida se redujo de escala micro a nanométrica, independientemente de la fuente de sinterización. Esta observación está respaldada por nuestros modelos matemáticos previamente publicados que establecen relaciones entre la permeabilidad magnética compleja, los mecanismos de magnetización, la frecuencia angular y la microestructura de la ferrita.

Introduction

EMI ferrites, also known as electromagnetic interference (EMI) suppression ferrites, are a type of magnetic material commonly used to suppress electromagnetic noise in electronic circuits. They are composed of ceramic ferrite materials, typically made of iron oxide mixed with other metals such as nickel, zinc, and manganese. EMI ferrites are characterized by their high permeability and magnetic loss, which allows them to effectively absorb and dissipate electromagnetic radiation [1,2]. They are widely used in applications such as power supplies, telecommunications, and automotive electronics to improve signal quality.

Among ferrites, Ni–Zn ferrite possesses the capability to absorb electromagnetic radiation at high frequencies, rendering it a suitable material for use as a magnetic absorber [3–12]. When electromagnetic waves encounter a ferrite absorber, they are converted into heat and dissipated throughout the material. As a result, the intensity of the electromagnetic wave diminishes, leading to the widespread utilization of Ni–Zn ferrite absorbers in electronic devices.

Ni–Zn ferrite absorbers can be produced from both microparticulated and nanoparticulated powders using a variety of methods, including microwave sintering. By controlling the grain size and distribution of the material, it is possible to produce absorbers with specific magnetic properties that are optimized for different applications. Absorbers could be designed to absorb specific frequencies or to provide broadband absorption across a range of frequencies [13–15].

Sintering is a key process in the production of NiZn ferrites, which involves the formation of a solid piece from a powdered material by heating it to a temperature below its melting point. The sintering process can affect the microstructure and properties of the final product, which, together with the chemical composition, determines its magnetic properties [3,4,16]. For instance, the addition of dopants such as Cu can enhance the magnetic properties of NiZn ferrites by reducing their grain size and improving their magnetic anisotropy [10,17,18].

Microwave sintering has emerged as a promising alternative to traditional sintering techniques, such as infrared conventional sintering, due to its ability to produce dense and homogeneous materials with reduced processing times and energy consumption [19,20]. Studies have shown that microwave sintering can improve the densification and microstructural homogeneity of NiZn ferrites, resulting in enhanced magnetic properties [21–25].

However, microwave sintering has some potential problems that need to be addressed in order to obtain optimal results [22,26]. Some common problems are: (i) uneven heating: if the microwave energy distribution is not uniform, the sample may heat unevenly, leading to non-uniform sintering and undesirable microstructures; (ii) overheating: overheating can lead to excessive grain growth, resulting in a reduction of

the desired magnetic properties; (iii) thermal runaway: this phenomenon can occur when the sample absorbs microwave energy more rapidly than it can dissipate heat. It can lead to an uncontrolled temperature increase and damage to the sample and equipment; (iv) thermal stresses: rapid heating and cooling can lead to thermal stresses that can cause cracking and other defects in the sintered material; (v) poor microwave absorption: some materials may not absorb microwave energy efficiently, resulting in poor sintering.

To overcome these problems, careful control of the sintering parameters, such as the heating rate, holding time, and power level, is necessary. It is also important to optimize the sample geometry, including the size and shape, to ensure uniform heating.

Nano ferrite sintering involves the consolidation of nanoparticulated powders into bulk materials through the application of heat and pressure. In this case, sintering is also a crucial step in the processing of nanoparticulated materials, as it determines the final microstructure, physical and chemical properties, and performance of the resulting bulk material. Traditional sintering techniques are often ineffective for nanoparticulated powders, as they require high temperatures and long sintering times that can lead to grain growth, agglomeration, and loss of desirable final properties. Therefore, novel sintering techniques, such as spark plasma sintering [27,28], microwave sintering [29,30], and pressureless sintering [31], will be developed to overcome these issues and produce high-quality nanostructured materials with tailored properties for various applications.

Sintering of nano-sized ferrite particles can be challenging due to several factors [32–34]. One of the main issues is achieving high densification levels and minimizing the porosity in the sintered material. Nanosized particles tend to have a high surface area to volume ratio, which makes them more prone to agglomeration and the formation of pores. The sintering process involves a complex mass transfer-controlling mechanisms during densification and grain growth [35] that can be affected by various factors such as particle parameters (size, shape and distribution), sintering temperature, sintering time, pressure, and atmosphere.

While some authors have explored microwave sintering of microparticulated NiZ ferrites to form bulk specimens [21,24,29], there is a dearth of research pertaining to the fabrication of these bulk soft ferrites from nanometric raw materials. Moreover, the conclusions drawn from the existing studies regarding the microstructural changes during the microwave sintering process exhibit discrepancies. In this study, microwave and traditional infrared sintering methods were used to sinter nano- and microstructured Ni–Zn ferrites doped with Cu. The morphology, microstructure, and magnetic properties of both granulometries were examined to explore the microstructural evolution during both sintering processes and to evaluate the implications of diminishing the raw material particle size from micro to nano. It was observed that microwave sintering improved the densification of both granulometries, reduced the average grain size of the microstructured ferrite, and increased that of the nanostructured one. In addition, the magnetic properties of the microstructured ferrite were improved by microwave sintering, while the magnetic permeability values of the microwave-sintered nanostructured ferrite were lower than that of the traditionally infrared-sintered ferrite, which would be further discussed.

Materials and methods

Micro- and nanostrucrured ferrites

Similar to previous publications [36,37], a polycrystalline ferrite material with a chemical composition of $(Cu_{0.12}Ni_{0.23}Zn_{0.65})Fe_2O_4$, supplied by Fair-Rite Products Corp., and an average size of 1–2 μm (Fig. 1) was used as the raw microparticulated starting powder (labeled as MICRO sample). The true density of the ferrite powder was determined to be 5380 kg/m^3 using a helium pycnometer.

The nanoparticulated starting powder was obtained from the MICRO sample using a top-down method, as detailed in a previous publication [38]. Briefly, the MICRO ferrite powder was ground for 2 h using a planetary ball mill and wet-milled for 48 h in a horizontal bead mill, using distilled water and zirconia balls. A 3 wt% ammonium polymethacrylate solution was used as a dispersing agent. The resulting milled powder (labeled as NANO sample) exhibited an average particle size of 25–30 nm (Fig. 1), determined from the specific surface area (SBET) measured by nitrogen adsorption using a MICROMERITICS TriStar 3000 instrument.

The crystal structure and crystallite size were determined by X-ray diffraction on a BRUKER D8 Advance diffractometer, and the morphological analysis of the particles was performed using a scanning electron microscopy (FEI Quanta 200 ESEM FEG microscope).

Shaping, sintering and characterization of ferrite specimens

Cylindrical and toroidal test specimens were prepared with a thickness of 3 mm and an external diameter of 19 mm. The toroidal specimens had an internal diameter of 6 mm. Toroidal specimens are essential for complex permeability measurements, designed to fit the sample holder. In contrast, cylindrical samples assess microstructural parameters like relative density (ϕ) and average grain size (G).

Starting powders were pressed using uniaxial (100 MPa) and isostatic (250 MPa) pressing methods to achieve a green relative density of 64% for the MICRO samples and 50% for the NANO samples. The specimens were sintered in air using either an infrared source (Carbolite® CWF13/13) or a 2.45 GHz microwave source (MKH-4.8 Linn High Therm GmbH) at sintering temperatures ranging from 900 °C to 1100 °C for 10 min.

Bulk density was determined using the Archimedes method, and the relative density (ϕ) was calculated as the ratio of bulk density to theoretical density. The average grain size (G) was obtained by scanning electron microscopy (SEM) image processing of the cylindrical test specimens using the ImageJ software, assuming that all grains were spherical. Over 1000 grains were measured for the characterization of each sample. Grain size distributions were obtained by plotting the accumulated frequency against diameter, with G representing

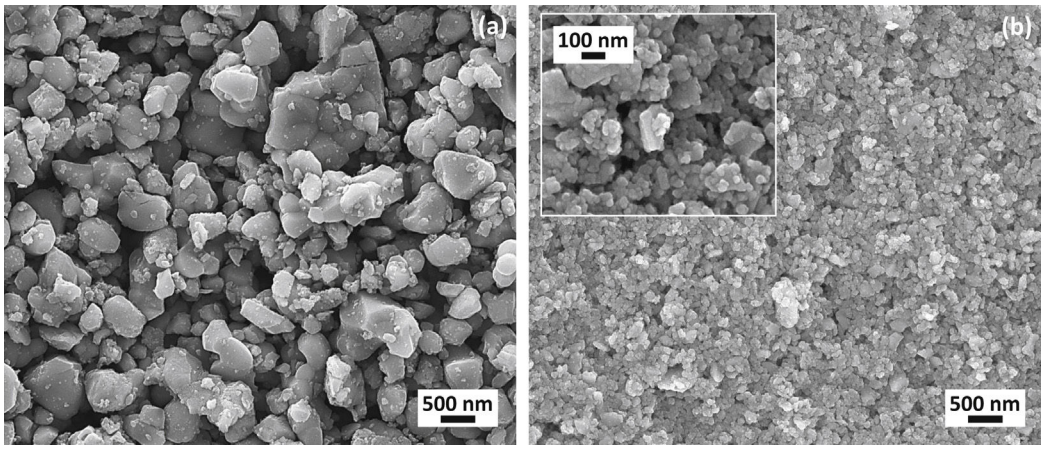

Fig. 1 – SEM micrographs of the (a) MICRO and (b) NANO ferrite starting powders.

the grain diameter at which 50% of the grains in area are smaller and S representing the width of the grain-size distribution. This width is defined as the difference between the grain size corresponding to 95 cumulative area percent finer (G_{95}) and the grain size corresponding to 5 cumulative area percent finer (G_5) in each specimen. The SEM micrographs presented in Fig. 1 depict platinum-coated samples, a process that tends to lend a more rounded and magnified appearance to the particles.

The real (μ') and imaginary (μ'') parts of the complex magnetic permeability were measured in the frequency range of 10^6–10^9 Hz using an Agilent E4991A RF impedance/material analyzer, along with an Agilent 16454A magnetic material test fixture.

Results and discussion

The NiZn(Fe_2O_4) ferrite was the only crystalline structure identified in both granulometries (MICRO and NANO). Fig. 2 shows the X-ray diffraction profiles of both starting powders observing a peak intensity decreased with granulometric reduction, which reflects the reduction in crystallite size as reported in a previously study [38]. Corresponding to that research, high-energy milling resulted in reductions in both crystallite size (from 68 to 11 nm) and particle size (from 1–2 μm to 25–30 nm). Additionally, there was a decline in the average number of aggregated crystallites per particle, dropping from 4 to 2 as observed in the same study.

Microwave sintering, compared to conventional infrared sintering, increases the densification of both ferrite granulometries studied, MICRO and NANO (Fig. 3 and Supplementary Table 1), as has been described by other authors [22–25,39,40]. Microwave radiation induces rapid and uniform heating within the material during the sintering process. Unlike infrared sintering and other heating methods, microwaves are absorbed by the material, enabling volumetric heating [29,41,42]. The efficient and precise heating of the ferrite particles within the microwave furnace enhances atom diffusion. Moreover, microwave sintering creates a concentrated and powerful microwave field surrounding the samples, surpassing the strength of the external field [43]. This concentration of the microwave field leads to ionization at the surface of ferrite particles, accelerating the diffusion of ions, and resulting in faster and more uniform densification. Our results confirm a more uniform densification in the case of the MICRO powder, as opposed to the NANO variant (Fig. 4), with a reduction in the width of the grain-size distribution observed for the MICRO sample (see Supplementary Fig. 1).

Fig. 5 depicts the EDX spectra of a sample with bright particles, similar to the ones observed in Fig. 4g, and a sample without them. The analysis suggests an incipient precipitated secondary phase rich in copper, which is almost indetectable and has no appreciable effect on the final properties of the ferrites, unlike those detected in preliminary studies [6,7]. These particles have only been detected in the MW sintering samples (both MICRO and NANO), suggesting an association with MW sintering.

As is well known, MW sintering directly couples ceramic powder parts to an electromagnetic or electrical power source, placing the heat source effectively within the bulk of the part. This approach, characterized by its energy efficiency, eliminates the need to heat an entire furnace, enabling faster sintering due to the low thermal inertia of the parts. However, MW sintering faces the challenge of so-called hot spots—localized overheating in certain regions of the heated specimen. This phenomenon results from concentrated coupling and heating, primarily driven by the high heating rates [44].

This localized overheating could be responsible for the detected copper-rich incipient phase, which, in this case, has not appeared to interfere with the final properties, as no differences have been observed compared to the IR samples.

Microwave sintering reduces the grain size of MICRO ferrites (Fig. 6) compared to IR sintering, as reported by other authors [21–23,25,39,40], and increases the grain size of NANO ferrites (Fig. 6), as also reported in the literature [24]. Grain refinement through microwave processing is typically attributed to the shorter sintering period [25], whereas grain growth is explained by the increase in the kinetic energy of ions at grain boundaries, which reduces the activation energy for forward ion diffusion and increases the barrier height for reverse diffusion [29]. Consequently, intergrain ion diffusion is facilitated, resulting in accelerated grain growth during sintering.

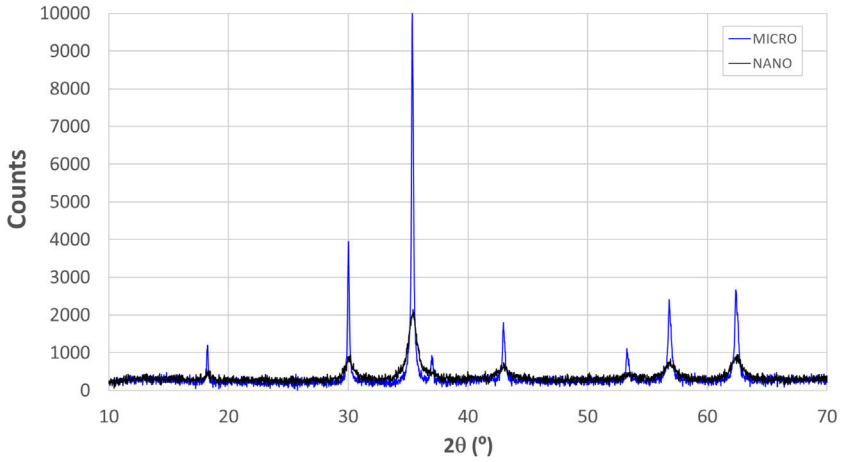

Fig. 2 – X-ray diffraction patterns of the MICRO and NANO starting powders corresponding to the crystal structure of NiZn(Fe_2O_4).

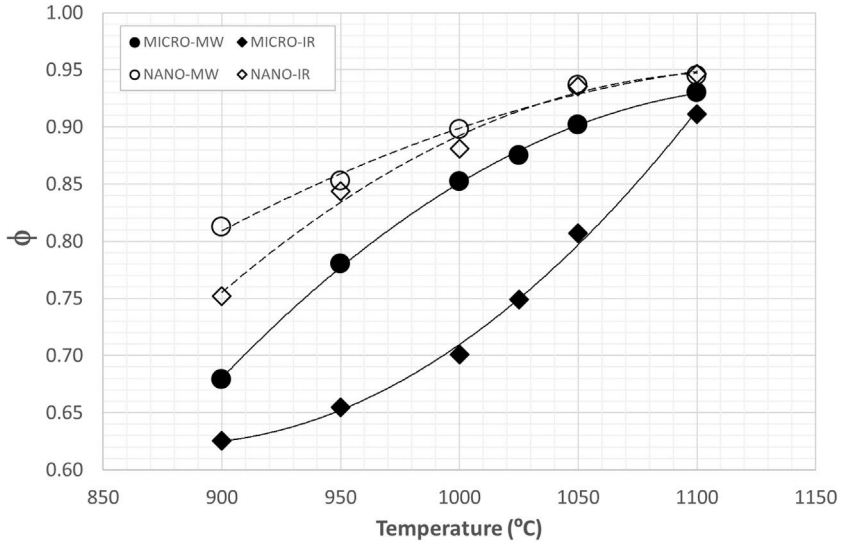

Fig. 3 – Temperature dependence of relative density for the two studied granulometries (MICRO and NANO) sintered with both infrared radiation (IR) and microwaves (MW).

In general, the high heating rates during microwave sintering facilitate the movement of the atoms, promoting their migration to grain boundaries and enabling diffusion across them. Nanosized ferrite powders, with their larger surface area and smaller particle size, exhibit faster atomic rearrangement and enhanced diffusion compared to microsized powders. Consequently, the final grain size distribution depends on a combination of sintering parameters, such as temperature and time. Since nanosized particles are more reactive and required shorter sintering times, using the same sintering parameters can result in different microstructure evolution behaviors compared to microsized particles. This could explain the observed differences in grain size evolution of the MICRO and NANO samples sintered under the same conditions. However, microwave sintering ensures uniform and homogeneous heating throughout the material, regardless of the particle size. The rapid and efficient heating provided by microwave sintering helps minimize temperature gradients, leading to improved homogeneity in the final sintered product (Fig. 4 and Supplementary Fig. 1).

In terms of the final properties (Fig. 7), microwave sintering enhances the magnetic properties of MICRO ferrites, reaching a higher value of the imaginary part (μ'') of the complex magnetic permeability. This improvement is achieved through enhanced densification and reduced grain size. However, microwave sintering does not lead to improved properties in the case of NANO ferrites, as they exhibit similar values to those achieved thorough conventional infrared sintering. The complete frequency dispersion spectra of the imaginary part (μ'') of the complex magnetic permeability of the MICRO and NANO microwave sintered samples are shown in Supplementary Fig. 2.

During the sintering process, two concurrent processes, densification and grain growth, occur in competition. These processes are interdependent and cannot be studied in isolation [35]. Together, they shape the final microstructure,

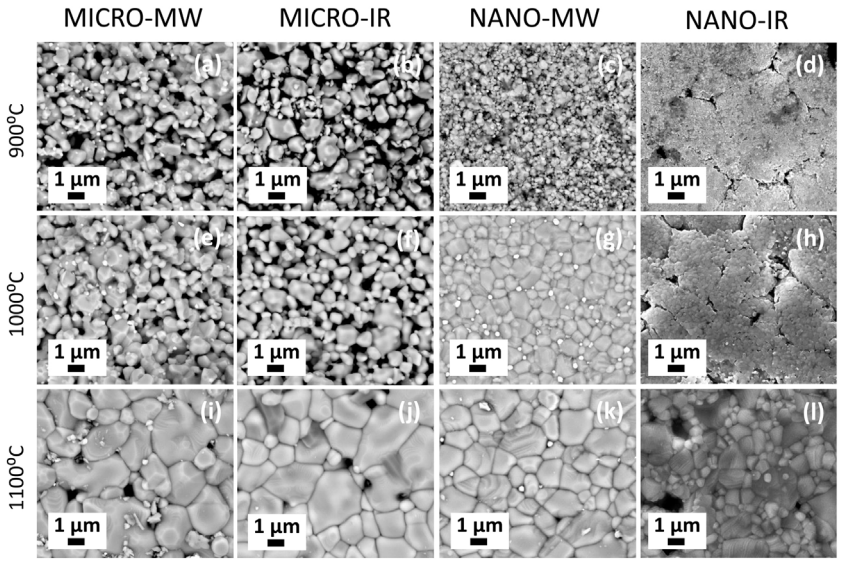

Fig. 4 – Scanning electron microscopy (SEM) images for the sintered MICRO-MW samples at 900 °C (a), 1000 °C (e) and 1100 °C (i); the MICRO-IR samples at 900 °C (b), 1000 °C (f) and 1100 °C (j); the NANO-MW samples at 900 °C (c), 1000 °C (g) and 1100 °C (k); and the NANO-IR samples at 900 °C (d), 1000 °C (h) and 1100 °C (l).

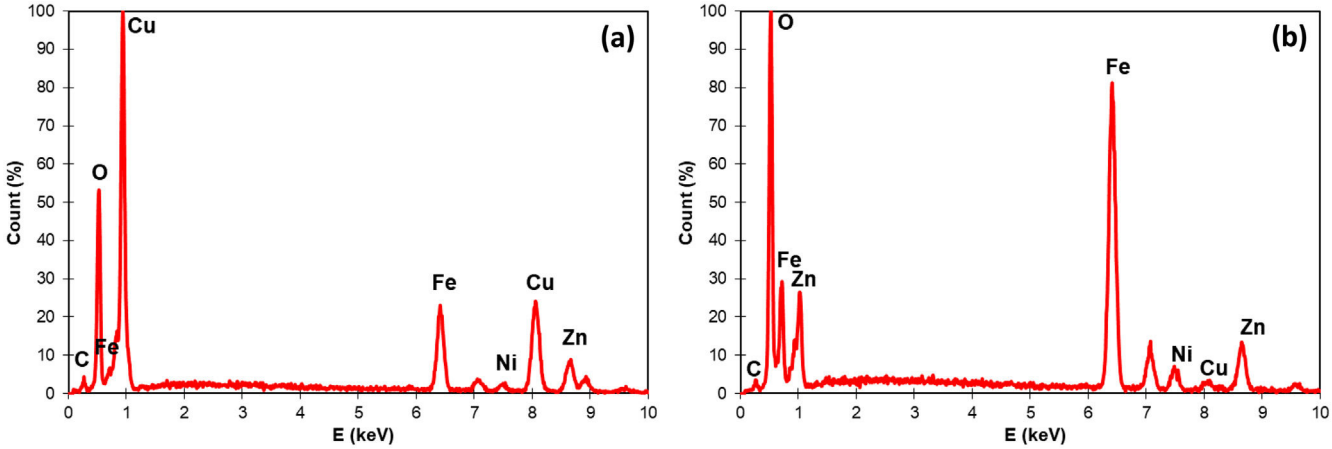

Fig. 5 – EDX spectra of a sample with bright particles (Fig. 4g) (a) and a sample without them (b).

which in turn governs the resulting electromagnetic properties [3–5,9,16,36,37,45–47]. Our findings demonstrate that MW sintering enhances densification while mitigating grain growth for MICRO ferrite powder. It's established that optimal electromagnetic results are achieved with higher densification (or lower porosity) and larger grain sizes [1], provided that a grain size limit is not exceeded [3]. As depicted in Fig. 7, the imaginary part (μ'') of the complex magnetic permeability improves with microwave sintering, reflecting an overall improvement in the final microstructure (higher ϕ and G). However, the most favorable outcome in this case corresponds to a pair of ϕ/G values where G is higher, primarily because the relative density value is also greater than that achieved with IR sintering. Similarly, NANO powder μ'' also benefits from increasing relative density and average grain size (Fig. 7). However, unlike the MICRO samples, the peak μ'' value achieved is noticeably lower. Even at the higher sintering temperature (1100 °C), improved sample densification is not observed; instead, it results in excessive grain growth, as indicated by the samples marked with an asterisk (*) in Fig. 7.

The improvement of μ'' observed with microwave sintering for the MICRO sample can be attributed to several factors. Microwave sintering promotes densification, reducing porosity and improving the packing density of the ferrite material. The rapid and volumetric heating provided by microwave radiation facilitates efficient diffusion of atoms, ions, and vacancies, providing better control over material composition homogeneity, impurity distribution, grain size consistency and uniform grain orientation [21,24,30,43]. The concentration of the intense microwave field around the samples during microwave sintering can also influence the alignment and movement of magnetic moments within the material. These factors collectively lead to an improved microstructure, better alignment of magnetic domains, reduction in the number of domain walls, and decreased losses associated with domain wall movement. As a result, the material's magnetic response to external fields is enhanced [21,48–50].

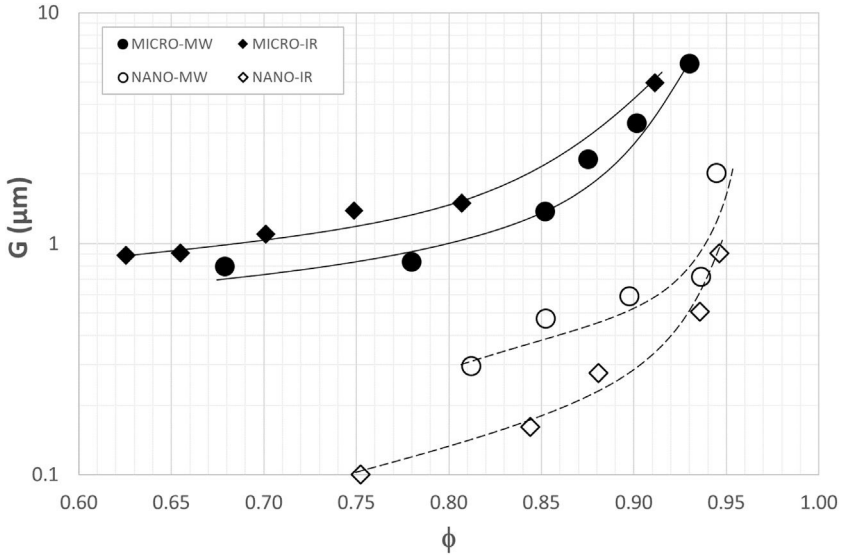

Fig. 6 – Relative density dependence of average grain size for the two studied granulometries (MICRO and NANO) sintered with both infrared radiation (IR) and microwaves (MW).

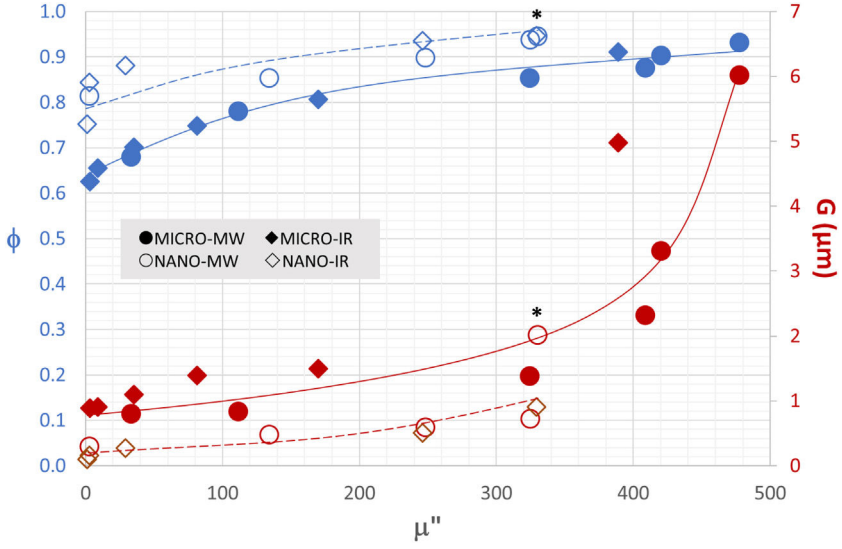

Fig. 7 – Imaginary part (μ'') of the complex magnetic permeability dependence of relative density (blue) and average grain size (red) for the two studied granulometries (MICRO and NANO) sintered with both infrared radiation (IR) and microwaves (MW).

As it well known, complex magnetic permeability has two contributions, the spin rotation mechanism, which describes the alignment of electron spins with an external magnetic field, and the domain-wall motion mechanism, which accounts for the movement of domain walls within a magnetic material [2,11,12,17,45,48,51–53]. In our previous work [5,54], we proposed and validated two mathematical models that capture the real (μ') and imaginary (μ'') components of the complex magnetic permeability while considering their dependence on microstructural factors. The imaginary (μ'') model (Eq. (1)) incorporates both physical mechanisms: spin rotation and domain-wall motion [54].

$$\mu'' = \mu''_S \cdot \psi + \mu''_{DW} \cdot \left(\frac{G^2}{b'' + G^2} \right) \cdot \psi \tag{1}$$

where μ''_S is the imaginary part-complex magnetic permeability spin rotation contribution and μ''_{DW} is the imaginary part-complex magnetic permeability domain-wall motion contribution (both are intrinsic values for a specific ferrite chemical composition at a given angular frequency).

In Eq. (1) ψ and b'' are defined as follows:

$$\psi = \frac{\phi - \phi_{lim}}{1 - \phi_{lim}} \tag{2}$$

$$b'' = 4\pi^2 d_w^2 \quad (3)$$

The concept of ψ becomes effective when comparing systems with different initial porosities. ϕ_{lim} (which is an empirical parameter) represents the minimum relative density value beyond which the chosen magnetic property is distinctly measurable, given the measurement's accuracy (for lower relative densities, magnetic permeability is virtually zero), and d_w refers to the domain-wall width [55].

The spin rotation contribution incorporates the relative density parameter, while the domain-wall motion contribution takes into account both the relative density and the average grain size. This explains the observed improvement in magnetic properties with microstructure enhancement in the MICRO samples.

Microstructure enhancement entails a densely sintered microstructure with low porosity, as well as a fine and precisely controlled grain size distribution [56]. Pores obstruct domain motion, reducing the demagnetization field [57,58]. It's also crucial to prevent residual porosity from becoming trapped within grains, often linked to large grain growth, as it hampers the magnetization process, resulting in lower permeability [59]. Both trapped pores and grain boundaries adversely affect electromagnetic properties, with grain boundaries acting as impurity sinks, concentrating structural disorders and non-magnetic phases, leading to a decrease in the initial effective permeability [36].

Furthermore, the results (Fig. 7) indicated that the imaginary part (μ'') of the complex magnetic permeability for NANO ferrite exhibits an increase with relative density and average grain size. However, it reaches a significantly lower maximum value compared to microferrite.

In previous studies we have seen how the magnetic permeability (μ'') increases in microparticulated ferrite sintered by IR as the average grain size (G) grows up to a critical value (approximately 20–25 μm) [36,37]. Beyond this threshold, the properties deteriorate significantly due to the presence of trapped pores within the grains and the formation of non-magnetic phases precipitated along the grain boundaries [6,7].

In this current study, we maintained homogeneous and normal grain growth for the MICRO ferrites, with grain size values below the limiting value (G_{lim}). As a result, an increase in μ'' with increasing G is observed throughout the entire interval, as shown in Fig. 7. However, for the NANO powder, as depicted in the same figure, even at higher sintering temperatures, both ϕ and μ'' do not improve, despite the larger grain size attained (see samples marked with an asterisk (*) in Fig. 7).

As previously discussed [54], the initial notion that ferrite nanoparticles exhibit superior electromagnetic properties compared to microparticles is contradicted when these nanoparticles undergo shaping and sintering. This counter-effect can be attributed to two primary factors:

i. Difficulty in achieving high densification values (ψ) when targeting relative density values (ϕ) above 0.96, despite a high ϕ_{lim} value (0.87 for nanoferrites, in contrast to 0.65 for microparticulated ferrites).
ii. Both ferrite nanoparticles and microparticles feature significant grain boundaries, but nanoferrites have a highly discontinuous boundary due to the presence of numerous very small pores within the porosity.

In the same study [54], it was shown that the magnetic permeability (μ'') for nanoferrites tends to approach approximately 350, in contrast to the reported value of around 550 for microsized ferrites. This difference can be attributed to the increased number of grain boundaries observed during the processing of ferrite nanopowders, and this effect has also been observed with MW sintering, as seen in Fig. 7.

The literature indicates that nanoparticles of NiZn ferrites exhibit better electromagnetic behavior compared to microparticles [60]. However, ceramic bodies made from nanopowders, despite their superior electromagnetic behavior, show a lower value for μ''. The reasons pointed out in literature are: the presence of surface effects, resulting from the higher surface area-to-volume ratio of nanoparticles, which can lead to increased porosity; the smaller grain size, which leads to a greater number of grain boundaries and a higher tendency to agglomerate during processing, potentially causing material inhomogeneity; the introduction of defects and disorder in the crystalline structure based on the specific nanoferrite production process used, among others. These factors result in the presence of barriers that hinder the movement of the magnetic domain walls, consequently diminishing the magnetic properties of the material.

The developed mathematical model presented in Eq. (1), validated for both microferrite and nanoferrite, confirmed the invariance of the intrinsic parameters μ''_S and μ''_{DW}. Remarkably, these parameters were founded to depend solely on the chemical composition, regardless of the size of the starting powder or the grain size of the sintered ceramic body. Additionally, the models required the determination of the relative density limit (ϕ_{lim}). Notably, the ϕ_{lim} value found for nanoferrite was significantly higher compared to that for microferrite. This disparity explains the challenge in achieving high relative density and densification values in sintered nanoferrite bodies. Consequently, a lower maximum value of μ'' is observed compared to microferrite. The same rationale can be applied to explain the lower values attained in this study with the NANO-MW samples.

The aforementioned model, which were validated for both micro [5] and nano [54] $Cu_{0.12}Ni_{0.23}Zn_{0.55}(Fe_2O_4)$ ferrites, and conventionally sintered by infrared, have been tested in this case to the ferrite samples sintered using microwaves. The models that were tested correspond to Eq. (4) for the microsized starting powder and Eq. (5) for the nanosized one. The results obtained for a frequency of 10 MHz are shown in Table 1.

$$\mu'' = 290.87 \cdot \psi + 324.28 \cdot \left(\frac{G^2}{1.35 + G^2}\right) \quad (4)$$

$$\mu'' = 290.87 \cdot \psi + 324.28 \cdot \left(\frac{G^2}{0.06 + G^2}\right) \quad (5)$$

As stated in a previous publication [3], the domain-wall width can be estimated from Pankerts' model [55] as $d_w = \sqrt{b''/4\pi^2}$, where the value of b'' in Eqs. (4) and (5) is 1.35 and 0.06 μm^2, respectively. It is remarkable that this value cannot

Table 1 – Microstructural and imaginary part (μ'') of the complex magnetic permeability values for the for MICRO-MW and NANO-MW samples, along with their estimation using Eqs. (4) and (5) respectively.

Sample	T (°C)	G (μm)	ϕ	ϕ_{lim}	ψ	S (μm)	μ''_{Exp}	μ''_{Model}
MICRO-MW	1050	3.31	0.90	0.65	0.71	3.67	420.9	414.0
	1100	6.02	0.93		0.80	6.23	477.9	482.8
NANO-MW	1050	0.71	0.94	0.87	0.54	0.71	325.1	312.7
	1100	2.01	0.94		0.54	2.51	330.5	328.7

be the same for both starting powders due to the reduction of the domain-wall width when transitioning from micro to nanosized powders. This reduction leads toa a decrease in the average grain size of the final samples, as shown in Table 1. The same behavior is observed for the relative density limit, suggesting that greater compactness is required when working with nanosized powders, as discussed in a recent work [54]. These conclusions also explain the decrease of the imaginary part (μ'') of the complex magnetic permeability value in nanosized starting powders, attributed to the presence of a large number of domain-walls in the samples, resulting in inferior final properties.

Despite these observations, both models accurately reproduce the experimental values and further support the previous statements, validating the extension of the proposed models to other sintering techniques.

The estimated values of the static susceptibility of the spin rotation (K_S) and the domain-wall motion (K_{DW}) were founded to be similar to those proposed in the literature for microsized NiZn ferrites sintered using both conventional infrared radiation [48,50,51,53] and microwave radiation [24]. It is important to note that previous studies on microwave sintering proposed slightly different values of K_S and K_{DW} for each sintering process, although these differences were minimal. The apparent distinction between the two processes can be attributed to the fact that their model did not incorporate microstructural parameters. However, in our case, the same model has been validated for different starting granulometries and sintering processes, indicating that K_S and K_{DW} are intrinsic parameters of the $Cu_{0.12}Ni_{0.23}Zn_{0.55}(Fe_2O_4)$ ferrite and independent of microstructure and frequency.

Conclusions

The properties (morphology, microstructure, and complex magnetic permeability) of a nickel–zinc ferrite ($(Cu_{0.12}Ni_{0.23}Zn_{0.65})Fe_2O_4$) after sintering at temperatures ranging from 900 to 1100 °C have been investigated. The ferrite was obtained in two forms: microparticulated ferrite (MICRO) from commercial material and nanoparticulated ferrite (NANO) through high energy milling of the former; and the impact of microwave heating (MW) on the sintering process was explored compared to traditional infrared sintering (IR).

Microwave sintering improved the densification of both granulometries and reduced the average grain size in the MICRO ferrite, while increasing it in the NANO ferrite. Additionally, microwave sintering enhanced the magnetic properties of the MICRO ferrite, despite the microwave-sintered NANO ferrite exhibiting lower magnetic permeability compared to the traditionally infrared-sintered ferrite. However, this behavior is consistent with the mathematical models previously proposed and validated for micro and nanometric ferrites using a sintering conventional method.

This study provides further evidence to support the applicability of these models to microwave sintering. The estimated values of the static susceptibility of spin rotation (K_S) and domain-wall motion (K_{DW}) were found to be similar to those obtained for conventional infrared sintering, whether it was applied to micro or nanosized ferrite. Therefore, the validity of these models can be extended regardless of the sintering source utilized, as well as the granulometry previously observed.

In conclusion, microwave sintering is a viable method for producing ferrite components as EMI suppressors, offering the advantage of time and energy savings. Moreover, it enhances the electromagnetic properties of the sintered bodies compared to conventional methods when using a microparticulated powder as the starting material.

Conflict of interests

The authors declare that they have no known competing financial interests or personal relationships that could have appeared to influence the work reported in this paper.

Acknowledgments

This research was partially supported by the Generalitat Valenciana, grant number CIAICO/2021/063 and by the Universitat Jaume I, grant number UJIB2020-13. Complex relative permeability determination was carried out at the central facilities (Servei Central d'Instrumentació Científica) of the Universitat Jaume I.

Appendix A. Supplementary data

Supplementary data associated with this article can be found, in the online version, at doi:10.1016/j.plantsci.2004.08.011.

REFERENCES

[1] A. Goldman, Modern Ferrite Technology, 2nd ed., Springer US, 2006, http://dx.doi.org/10.1017/CBO9781107415324.004.
[2] T. Tsutaoka, Frequency dispersion of complex permeability in Mn–Zn and Ni–Zn spinel ferrites and their composite materials, J. Appl. Phys. 39 (2003) 2789–2796, http://dx.doi.org/10.1063/1.1542651.

[3] A. Barba, C. Clausell, J.C. Jarque, L. Nuño, Magnetic complex permeability (imaginary part) dependence on the microstructure of a Cu-doped Ni–Zn-polycrystalline sintered ferrite, Ceram. Int. 46 (2020) 14558–14566, http://dx.doi.org/10.1016/j.ceramint.2020.02.255.
[4] A. Barba-Juan, N. Vicente, A. Mormeneo-Segarra, C. Clausell-Terol, Influence of microstructure and magnetizing mechanisms on magnetic complex permeability (imaginary part) of a Cu-doped Ni–Zn polycrystalline ferrite, Ceram. Int. (2021), http://dx.doi.org/10.1016/j.ceramint.2021.07.119.
[5] A. Barba-Juan, A. Mormeneo-Segarra, N. Vicente, J.C. Jarque, C. Clausell-Terol, Frequency dispersion model of the complex permeability of soft ferrites in the microwave frequency range, J. Am. Ceram. Soc. 105 (2022) 2725–2734, http://dx.doi.org/10.1111/jace.18267.
[6] A. Barba, C. Clausell, L. Nuño, J.C. Jarque, ZnO and CuO crystal precipitation in sintering Cu-doped Ni–Zn ferrites, II. Influence of sintering temperature and sintering time, J. Eur. Ceram. Soc. 37 (2017) 169–177, http://dx.doi.org/10.1016/j.jeurceramsoc.2016.07.033.
[7] A. Barba, C. Clausell, J.C. Jarque, M. Monzó, ZnO and CuO crystal precipitation in sintering Cu-doped Ni–Zn ferrites, I. Influence of dry relative density and cooling rate, J. Eur. Ceram. Soc. 31 (2011) 2119–2128, http://dx.doi.org/10.1016/j.jeurceramsoc.2011.05.007.
[8] M. Manjurul Haque, M. Huq, M.A. Hakim, Influence of CuO and sintering temperature on the microstructure and magnetic properties of Mg–Cu–Zn ferrites, J. Magn. Magn. Mater. 320 (2008) 2792–2799, http://dx.doi.org/10.1016/j.jmmm.2008.06.017.
[9] A.C.F.M.F.M. Costa, E. Tortella, M.R. Morelli, R.H.G.A.G.A. Kiminami, Synthesis, microstructure and magnetic properties of Ni–Zn ferrites, J. Magn. Magn. Mater. 256 (2003) 174–182, http://dx.doi.org/10.1016/S0304-8853(02)00449-3.
[10] M.F. Huq, D.K. Saha, R. Ahmed, Z.H. Mahmood, Ni–Cu–Zn ferrite research: a brief review, J. Sci. Res. 5 (2013) 215–234, http://dx.doi.org/10.3329/jsr.v5i2.12434.
[11] O.F. Caltun, L. Spinu, A. Stancu, L.D. Thung, W. Zhou, Study of the microstructure and of the permeability spectra of Ni–Zn–Cu ferrites, J. Magn. Magn. Mater. 242–245 (2002) 160–162, http://dx.doi.org/10.1016/S0304-8853(01)01187-8.
[12] K. Kawano, N. Sakurai, S. Kusumi, H. Kishi, Magnetic permeability and microstructure of the Bi,Si oxides-doped NiZnCu ferrite composite material, J. Magn. Magn. Mater. 297 (2006) 26–32, http://dx.doi.org/10.1016/j.jmmm.2005.01.033.
[13] A.N. Yusoff, M.H. Abdullah, S.H. Ahmad, S.F. Jusoh, A.A. Mansor, S.A.A. Hamid, Electromagnetic and absorption properties of some microwave absorbers, J. Appl. Phys. 92 (2002) 876–882, http://dx.doi.org/10.1063/1.1489092.
[14] M. Derakhshani, E. Taheri-Nassaj, M. Jazirehpour, S.M. Masoudpanah, Enhanced electromagnetic wave absorption performance of Ni–Zn ferrite through the added structural macroporosity, J. Mater. Res. Technol. 16 (2022) 700–714, http://dx.doi.org/10.1016/j.jmrt.2021.12.026.
[15] M. Pardavi-Horvath, Microwave applications of soft ferrites, J. Magn. Magn. Mater. 215 (2000) 171–183, http://dx.doi.org/10.1016/S0304-8853(00)00106-2.
[16] C. Clausell-Terol, A. Barba-Juan, L. Nuño, Sintered microstructure effect on RF-wave shielding properties of a Cu-doped Ni–Zn-polycrystalline ferrite, Bol. Soc. Esp. Ceram. Vidr. 62 (2023) 108–122, http://dx.doi.org/10.1016/j.bsecv.2021.09.006.
[17] T. Nakamura, Low-temperature sintering of Ni–Zn–Cu ferrite and its permeability spectra, J. Magn. Magn. Mater. 168 (1997) 285–291, http://dx.doi.org/10.1016/S0304-8853(96)00709-3.
[18] M.P. Reddy, W. Madhuri, N.R. Reddy, K.V.S. Kumar, V.R.K. Murthy, R.R. Reddy, Influence of copper substitution on magnetic and electrical properties of MgCuZn ferrite prepared by microwave sintering method, Mater. Sci. Eng. C 30 (2010) 1094–1099, http://dx.doi.org/10.1016/j.msec.2010.06.002.
[19] J. Lasri, P.D. Ramesh, L. Schächter, Energy conversion during microwave sintering of a multiphase ceramic surrounded by a susceptor, J. Am. Ceram. Soc. 83 (2000) 1465–1468, http://dx.doi.org/10.1111/j.1151-2916.2000.tb01411.x.
[20] A. Chatterjee, T. Basak, K.G. Ayappa, Analysis of microwave sintering of ceramics, AIChE J. 44 (1998) 2302–2311.
[21] Y.J. Yang, C.I. Sheu, S.Y. Cheng, H.Y. Chang, Si-Ca species modification and microwave sintering for NiZn ferrites, J. Magn. Magn. Mater. 284 (2004) 220–226, http://dx.doi.org/10.1016/j.jmmm.2004.06.040.
[22] M. Sorescu, L. Diamandescu, R. Peelamedu, R. Roy, P. Yadoji, Structural and magnetic properties of NiZn ferrites prepared by microwave sintering, J. Magn. Magn. Mater. 279 (2004) 195–201, http://dx.doi.org/10.1016/j.jmmm.2004.01.079.
[23] C.Y. Tsay, K.S. Liu, I.N. Lin, Co-firing process using conventional and microwave sintering technologies for MnZn- and NiZn-ferrites, J. Eur. Ceram. Soc. 21 (2001) 1937–1940, http://dx.doi.org/10.1016/S0955-2219(01)00146-7.
[24] M. Yan, J. Hu, Microwave sintering of high-permeability $(Ni_{0.20}Zn_{0.60}Cu_{0.20})Fe_{1.98}O_4$ ferrite at low sintering temperatures, J. Magn. Magn. Mater. 305 (2006) 171–176, http://dx.doi.org/10.1016/j.jmmm.2005.12.008.
[25] M. Maisnam, S. Phanjoubam, P. Kumar, J.K. Juneja, A. Kumar, C. Prakash, Improved properties of Li–Mn–Ti ferrites by microwave sintering, Integr. Ferroelectr. 122 (2010) 31–37, http://dx.doi.org/10.1080/10584587.2010.504397.
[26] T. Saji, Microwave sintering of large products, MRS Online Proc. Libr. 430 (1996) 15–20, http://dx.doi.org/10.1557/PROC-430-15.
[27] S. Song, Q. Song, J. Li, V.R. Mudinepalli, Z. Zhang, Characterization of submicrometer-sized NiZn ferrite prepared by spark plasma sintering, Ceram. Int. 40 (2014) 6473–6479, http://dx.doi.org/10.1016/j.ceramint.2013.11.099.
[28] J. Sun, J. Li, G. Sun, W. Qu, Synthesis of dense NiZn ferrites by spark plasma sintering, Ceram. Int. 28 (2002) 855–858, http://dx.doi.org/10.1016/S0272-8842(02)00064-0.
[29] P. Yadoji, R. Peelamedu, D. Agrawal, R. Roy, Microwave sintering of Ni–Zn ferrites: comparison with conventional sintering, Mater. Sci. Eng. B Solid-State Mater. Adv. Technol. 98 (2003) 269–278, http://dx.doi.org/10.1016/S0921-5107(03)00063-1.
[30] M. Penchal Reddy, W. Madhuri, G. Balakrishnaiah, N. Ramamanohar Reddy, K.V. Siva Kumar, V.R.K. Murthy, R. Ramakrishna Reddy, Microwave sintering of iron deficient Ni–Cu–Zn ferrites for multilayer chip inductors, Curr. Appl. Phys. 11 (2011) 191–198, http://dx.doi.org/10.1016/j.cap.2010.07.005.
[31] A. Stratta, B. Ahmadi, B. Mouawad, S. Robertson, L. De Lillo, L. Empringham, M. Johnson, 3D structure design of magnetic ferrite cores using gelcasting and pressure-less sintering process, AIP Adv. 9 (2019), http://dx.doi.org/10.1063/1.5080008.
[32] A. Gholizadeh, E. Jafari, Effects of sintering atmosphere and temperature on structural and magnetic properties of Ni–Cu–Zn ferrite nano-particles: magnetic enhancement by a reducing atmosphere, J. Magn. Magn. Mater. 422 (2017) 328–336, http://dx.doi.org/10.1016/j.jmmm.2016.09.029.
[33] Y.B. Kannan, R. Saravanan, N. Srinivasan, I. Ismail, Sintering effect on structural, magnetic and optical properties of $Ni_{0.5}Zn_{0.5}Fe_2O_4$ ferrite nano particles, J. Magn. Magn. Mater. 423 (2017) 217–225, http://dx.doi.org/10.1016/j.jmmm.2016.09.038.
[34] M.M. Kothawale, R.B. Tangsali, S.S. Meena, N.K. Prasad, A. Gangwar, Mössbauer study and curie temperature configuration on sintering nano-Ni–Zn ferrite powder, J.

Supercond. Nov. Magn. 32 (2019) 2141–2147, http://dx.doi.org/10.1007/s10948-018-4935-x.
[35] A. Barba-Juan, C. Clausell-Terol, A general method to determine optimal thermal cycles based on solid-state sintering fundamentals, Ceram. Int. 45 (2019) 5346–5354, http://dx.doi.org/10.1016/j.ceramint.2018.11.233.
[36] C. Clausell, A. Barba, L. Nuño, J.C. Jarque, Effect of average grain size and sintered relative density on the imaginary part – μ'' of the complex magnetic permeability of $(Cu_{0.12}Ni_{0.23}Zn_{0.65})Fe_2O_4$ system, Ceram. Int. 42 (2016) 4256–4261, http://dx.doi.org/10.1016/j.ceramint.2015.11.101.
[37] C. Clausell, A. Barba, L. Nuño, J.C. Jarque, Electromagnetic properties of ferrite tile absorber as a function of compaction pressure, Ceram. Int. 42 (2016) 17303–17309, http://dx.doi.org/10.1016/j.ceramint.2016.08.026.
[38] A. Barba, C. Clausell, J.C.J.C. Jarque, M. Monzó, Obtainment of nanoparticulate CuNiZn ferrite powder by high-energy milling, J. Ceram. Soc. Jpn. 120 (2012) 311–316, http://dx.doi.org/10.2109/jcersj2.120.311.
[39] C.Y. Tsay, K.S. Liu, T.F. Lin, I.N. Lin, Microwave sintering of NiCuZn ferrites and multilayer chip inductors, J. Magn. Magn. Mater. 209 (2000) 189–192, http://dx.doi.org/10.1016/S0304-8853(99)00684-8.
[40] D.E. Clark, D.C. Folz, J.K. West, Processing materials with microwave energy, Mater. Sci. Eng. A 287 (2000) 153–158, http://dx.doi.org/10.1016/s0921-5093(00)00768-1.
[41] A.R. Phani, S. Santucci, Evaluation of structural and mechanical properties of aluminum oxide thin films deposited by a sol–gel process: comparison of microwave to conventional anneal, J. Non. Cryst. Solids 352 (2006) 4093–4100, http://dx.doi.org/10.1016/j.jnoncrysol.2006.06.013.
[42] M. Penchal Reddy, W. Madhuri, N. Ramamanohar Reddy, K.V. Siva Kumar, V.R.K. Murthy, R. Ramakrishna Reddy, Magnetic properties of Ni–Zn ferrites prepared by microwave sintering method, J. Electroceramics 28 (2012) 1–9, http://dx.doi.org/10.1007/s10832-011-9670-7.
[43] D.C. Dube, P.D. Ramesh, J. Cheng, M.T. Lanagan, D. Agrawal, R. Roy, Experimental evidence of redistribution of fields during processing in a high-power microwave cavity, Appl. Phys. Lett. 85 (2004) 3632–3634, http://dx.doi.org/10.1063/1.1806542.
[44] J.-M. Chaix, R. Bouchet, D. Bouvard, T. Fabre, T. Garnault, C. Harnois, K. Koutoati, M. Lachal, S. Marinel, M.C. Steil, A viewpoint on hot spots in microwave sintering and flash sintering, Adv. Eng. Mater. 2 (2023) 2201742, http://dx.doi.org/10.1002/adem.202201742.
[45] H. Su, H. Zhang, X. Tang, Y. Jing, Z. Zhong, Complex permeability and permittivity spectra of polycrystalline Ni–Zn ferrite samples with different microstructures, J. Alloys Compd. 481 (2009) 841–844, http://dx.doi.org/10.1016/j.jallcom.2009.03.133.
[46] K. Kawano, M. Hachiya, Y. Iijima, N. Sato, Y. Mizuno, The grain size effect on the magnetic properties in NiZn ferrite and the quality factor of the inductor, J. Magn. Magn. Mater. 32 (2009) 2488–2493, http://dx.doi.org/10.1016/j.jmmm.2009.03.015.
[47] T. Jahanbin, M. Hashim, K. Amin Mantori, Comparative studies on the structure and electromagnetic properties of Ni–Zn ferrites prepared via co-precipitation and conventional ceramic processing routes, J. Magn. Magn. Mater. 322 (2010) 2684–2689, http://dx.doi.org/10.1016/j.jmmm.2010.04.008.
[48] T. Tsutaoka, M. Ueshima, T. Tokunaga, T. Nakamura, K. Hatakeyama, Frequency dispersion and temperature variation of complex permeability of Ni–Zn ferrite composite materials, J. Appl. Phys. 78 (1995) 3983–3991, http://dx.doi.org/10.1063/1.359919.
[49] A. Globus, P. Duplex, M. Guyot, Determination of initial magnetization curve from crystallites size and effective anisotropy field, IEEE Trans. Magn. 7 (1971) 617–622, http://dx.doi.org/10.1109/TMAG.1971.1067200.
[50] J. Hu, M. Yan, W. Luo, Preparation of high-permeability NiZn ferrites at low sintering temperatures, Phys. B Condens. Matter. 368 (2005) 251–260, http://dx.doi.org/10.1016/j.physb.2005.07.019.
[51] T. Nakamura, Study on High-Frequency Permeability in Ferrite Ceramics and Ferrite Composite Materials, Hiroshima University, 1996.
[52] W.G. Fano, S. Boggi, A.C. Razzitte, Causality study and numerical response of the magnetic permeability as a function of the frequency of ferrites using Kramers–Kronig relations, Phys. B Condens. Matter. 403 (2008) 526–530, http://dx.doi.org/10.1016/j.physb.2007.08.218.
[53] T. Nakamura, T. Tsutaoka, K. Hatakeyama, Frequency dispersion of permeability in ferrite composite materiales, J. Magn. Magn. Mater. 138 (1994) 319–328, http://dx.doi.org/10.1016/0304-8853(94)90054-X.
[54] A. Barba-Juan, N. Vicente, A. Mormeneo-Segarra, C. Clausell-Terol, Microstructure-dependent magnetic permeability in ferrites from nanoparticles, Ceram. Int. 49 (2023) 21530–21537, http://dx.doi.org/10.1016/j.ceramint.2023.03.287.
[55] J. Pankert, Influence of grain boundaries on complex permeability in MnZn ferrites, J. Magn. Magn. Mater. 138 (1994) 45–51, http://dx.doi.org/10.1016/0304-8853(94)90397-2.
[56] C. Clausell, A. Barba, Processing-microstructure-properties relationship in a CuNiZn ferrite, Bol. Soc. Esp. Ceram. Vidr. 57 (2018) 29–39, http://dx.doi.org/10.1016/j.bsecv.2017.09.002.
[57] A. Verma, T.C. Goel, R.G. Mendiratta, Frequency variation of initial permeability of NiZn ferrites prepared by the citrate precursor method, J. Magn. Magn. Mater. 210 (2000) 274–278, http://dx.doi.org/10.1016/S0304-8853(99)00451-5.
[58] J.J. Shrotri, S.D. Kulkarni, C.E. Deshpande, A. Mitra, S.R. Sainkar, P.S. Anil Kumar, S.K. Date, Effect of Cu substitution on the magnetic and electrical properties of Ni–Zn ferrite synthesised by soft chemical method, Mater. Chem. Phys. 59 (1999) 1–5, http://dx.doi.org/10.1016/S0254-0584(99)00019-X.
[59] J. Jeong, H.H. Han, B.C. Moon, Effects of Bi_2O_3 addition on the microstructure and electromagnetic properties of NiCuZn ferrites, J. Mater. Sci. Mater. Electron. 15 (2004) 303–306, http://dx.doi.org/10.1023/B:JMSE.0000024230.90882.ff.
[60] W. Wang, Z. Ding, X. Zhao, S. Wu, F. Li, M. Yue, J.P. Liu, Microstructure and magnetic properties of MFe_2O_4 (M = Co, Ni, and Mn) ferrite nanocrystals prepared using colloid mill and hydrothermal method, J. Appl. Phys. 117 (2015), http://dx.doi.org/10.1063/1.4917463.